

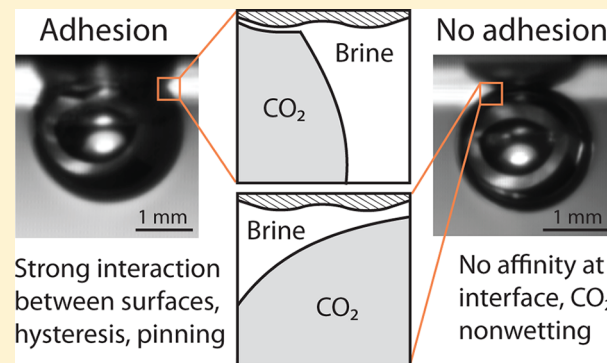
## CO<sub>2</sub> Adhesion on Hydrated Mineral Surfaces

Shibo Wang, Zhiyuan Tao, Sara M. Persily, and Andres F. Clarens\*

Civil and Environmental Engineering, Thornton Hall, University of Virginia, 351 McCormick Road, Charlottesville, Virginia 22904, United States

### Supporting Information

**ABSTRACT:** Hydrated mineral surfaces in the environment are generally hydrophilic but in certain cases can strongly adhere CO<sub>2</sub>, which is largely nonpolar. This adhesion can significantly alter the wettability characteristics of the mineral surface and consequently influence capillary/residual trapping and other multiphase flow processes in porous media. Here, the conditions influencing adhesion between CO<sub>2</sub> and homogeneous mineral surfaces were studied using static pendant contact angle measurements and captive advancing/receding tests. The prevalence of adhesion was sensitive to both surface roughness and aqueous chemistry. Adhesion was most widely observed on phlogopite mica, silica, and calcite surfaces with roughness on the order of ~10 nm. The incidence of adhesion increased with ionic strength and CO<sub>2</sub> partial pressure. Adhesion was very rarely observed on surfaces equilibrated with brines containing strong acid or base. In advancing/receding contact angle measurements, adhesion could increase the contact angle by a factor of 3. These results support an emerging understanding of adhesion of, nonpolar nonaqueous phase fluids on mineral surfaces influenced by the properties of the electrical double layer in the aqueous phase film and surface functional groups between the mineral and CO<sub>2</sub>.



equilibrated with brines containing strong acid or base. In advancing/receding contact angle measurements, adhesion could increase the contact angle by a factor of 3. These results support an emerging understanding of adhesion of, nonpolar nonaqueous phase fluids on mineral surfaces influenced by the properties of the electrical double layer in the aqueous phase film and surface functional groups between the mineral and CO<sub>2</sub>.

## INTRODUCTION

The wettability of aqueous and nonaqueous fluids on solid surfaces has a well-established impact on the transport of multiple phases through porous media.<sup>1</sup> The specific case of a hydrated mineral surface in contact with a hydrophobic nonaqueous phase fluid is relevant to a number of applications related to energy and/or the environment such as geologic carbon sequestration (GCS), enhanced oil recovery, and hydraulic fracturing of shales.<sup>2,3</sup> At the surface, most minerals contain hydroxyl functional groups (e.g.,  $\equiv\text{Al}-\text{OH}$  and  $\equiv\text{Si}-\text{OH}$ ) in equilibrium with the aqueous phase so that under conditions in which nonaqueous species (e.g., CO<sub>2</sub>, oil, or CH<sub>4</sub>) contact the surface, it would be expected to maintain its water-wetting characteristics.<sup>4</sup> Most work has suggested that differences in the solution chemistry (e.g., pH, ionic strength) and the mineral composition at the pore surface (e.g., quartz, kaolinite, silica, calcite) could lead to minor differences in wettability.<sup>5,6</sup> These changes would manifest on macro-scale flow properties like capillary pressure and residual saturation but are unlikely to change transport behavior dramatically.<sup>7</sup>

A growing number of studies investigating the CO<sub>2</sub>-brine-mineral interface have reported that more complex interfacial behavior can occur under certain circumstances.<sup>8–10</sup> Most of these studies describe wettability alteration caused by either contact line pinning or wettability hysteresis.<sup>2</sup> Contact line pinning occurs on certain minerals such as phlogopite mica and calcite when the ternary phase line between mineral, CO<sub>2</sub>, and brine stays fixed even under dynamic conditions (i.e., the droplet is growing or shrinking) and consequently, there is a

marked change in contact angle ( $\Theta$ ).<sup>8,9</sup> The pinned contact line represents a high energy barrier locally.<sup>11</sup> Wettability hysteresis occurs over time as chemical reactions, surface roughness or other characteristics at the surface lead to path dependent wetting behavior.<sup>12</sup> Both of these processes have been found to be most pronounced on micas which tend to form very smooth surfaces because of their monoclinic basal structure.<sup>13</sup> Other studies have explored the effect of salinity, which typically enhanced these effects, and pressure, which was also positively correlated with these wettability alterations.<sup>9</sup>

Recent work has indicated that interfacial (dispersive) adhesion could be the mechanism underlying or contributing to both pinning and hysteresis in these systems.<sup>10</sup> Adhesion is the manifestation of molecular affinity at the nanometer scale between dissimilar surfaces and is most often used to describe interfacial forces holding together ultra smooth solid surfaces in close contact (~10s of nanometers).<sup>14</sup> The adhesion force consists of both Lifshitz-van der Waals forces and electrostatic forces. Lifshitz-van der Waals forces are comprised of permanent dipole (Keesom) forces, dipole-induced dipole (Debye) forces, and dispersion (London) forces.<sup>15</sup> Lifshitz-van der Waals force can be described by Derjaguin, Landau, Verwey and Overbeek (DLVO) theory whereas the electrostatic force can be calculated with the linearized Poisson-Boltzmann

Received: May 16, 2013

Revised: August 28, 2013

Accepted: September 16, 2013

Published: September 16, 2013



ACS Publications

© 2013 American Chemical Society

11858

dx.doi.org/10.1021/es402199e | Environ. Sci. Technol. 2013, 47, 11858–11865

equation.<sup>16</sup> For the CO<sub>2</sub>-brine-mineral system, the Lifshitz-van der Waals force is equivalent to the disjoining pressure of the thin adsorbed water film separating the CO<sub>2</sub> from the mineral.<sup>17</sup> Disjoining pressure represents the change in excess Gibbs free energy (or Helmholtz free energy) and chemical potential per unit area of the film with respect to the film thickness, so the force is also a function of the thickness of the film.<sup>18</sup> CO<sub>2</sub> molecules are nonpolar but they have a permanent quadrupole moment that could result in attraction to mineral surfaces via these van der Waals forces, particularly London forces. The electrostatic forces are strongly affected by the properties of the solid surface and the vicinal fluids, for example, surface charge density and electronegativity. The relative importance of Lifshitz-van der Waals forces or electrostatic forces is influenced by pH and salinity.

A mechanistic understanding of adhesion between a nonpolar, nonaqueous liquid and a mineral surface on a hydrated mineral surface is somewhat complicated by the thin water film that could exist between the nonaqueous phase and the mineral surface.<sup>19</sup> This water layer has been found to be of great importance in the oil-brine-mineral system. Buckley et al. demonstrated the relationship between wettability, adhesion, and water layer structure for the purposes of crude oil extraction.<sup>20</sup> They suggest that adhesion can be explained using a combination of electrical double layer (EDL) calculations and a model of the ionizable surface group. Wettability of the mineral surface could be altered when the water layer at the interface was modified, and this could be achieved in several ways including by introducing acid/base to the system, which collapses the double layer and provides a strong charge imbalance at the surface. The water layer can also be significantly compressed by increasing the ionic strength of the aqueous phase. Based on this understanding, they achieved dramatic shifts in the wettability of quartz and were able to map the effects of pH and ionic strength on adhesion over a wide range of conditions. Despite the fact that the brine-mineral interface interacts differently with CO<sub>2</sub> than it does with oil, primarily because of the much higher solubility of water in CO<sub>2</sub> and creation of carbonate and bicarbonate ions, similar behaviors have been observed at the interface.

Both the density and speciation of hydroxyl groups at the mineral surface play important roles in controlling properties of the EDL and, by extension, the degree to which the nonaqueous phase will interact with the mineral surface.<sup>21</sup> Higher density of hydroxyl groups at the surface will create a more hydrophilic interface in the air-water system.<sup>22</sup> If the nonaqueous phase is CO<sub>2</sub>, it will interact with the surface in specific ways, contacting certain hydroxyl groups that are inaccessible to water, which will enable more intimate interactions with the bulk CO<sub>2</sub> phase.<sup>23</sup> Tripp and Combs used infrared spectroscopy to study the weak physisorption of CO<sub>2</sub> with surface hydroxyl function groups (silanols) on silica.<sup>24</sup> In separate work, this group studied the three main types of silanols, that is, isolated, hydrogen bonded and inaccessible silanols on silica and reported that CO<sub>2</sub> penetrates the regions containing inaccessible silanols which originally do not participate in interfacial reactions.<sup>23</sup> These observations were confirmed with molecular dynamic simulations.<sup>25,26</sup> They attribute wettability hysteresis to instability in the retreating/rupturing water film caused by CO<sub>2</sub>. They also observed that the interaction between CO<sub>2</sub> and surface hydroxyls is more prominent when the density of hydroxyl groups on the surface is high.<sup>24</sup> Hydroxyl groups at the surface can also be strongly

impacted by pH in solution and this will influence the extent to which the surface will react with aqueous CO<sub>2</sub>.

The water film at the CO<sub>2</sub>-brine-mineral interface is also impacted by surface roughness of the mineral. Surface roughness has been widely acknowledged to impact wettability hysteresis.<sup>27–29</sup> Generally, surface roughness below some threshold value (e.g., 10 μm) is considered negligible in contact angle experiments when drops are several mm in diameter.<sup>30</sup> But when adhesion is possible, surface roughness becomes much more important because it enables the wetting phase (in this case brine) to accumulate in surface asperities and prevents the short-range molecular forces that drive adhesion. This is not unlike two solid surfaces coming into contact with each other. If the surfaces are not polished enough to permit molecular interfacial forces, adhesion will not occur. This is illustrated in Figure 1 where the relative magnitude of

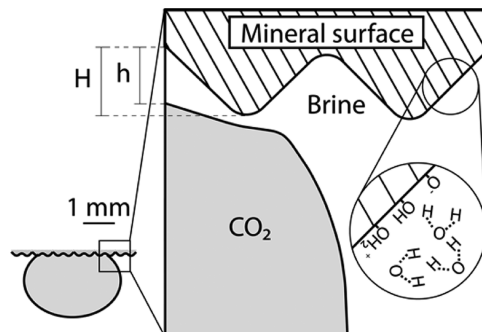


**Figure 1.** Schematic of the CO<sub>2</sub>-brine-mineral interface. The relative thickness of the water film (h) and the surface asperities (H) on the mineral surface impact the prevalence of adhesion. Solution chemistry also has an important effect on controlling the surface charge (round inset) and electrical double layer structure.

the water film thickness (h) and the surface asperities (H) will impact the ability of water to pool between protruding regions of the mineral surface, effectively preventing adhesive contact. The exact thickness of h has been widely studied and is believed to be on the order of 1–30 nm.<sup>31</sup>

The properties of the EDL and the speciation of hydroxyl groups are impacted by the chemistry of the aqueous phase. Under neutral pH conditions, or those near the pH point of zero charge (pH<sub>pzc</sub>) for a mineral surface, the concentration of anions and cations at the surface is nearly equivalent. Large swings in pH can restructure the distribution of surface charges. A number of groups have reported on the rearrangement of the interfacial water network on a mineral surface as a result of pH conditions in the aqueous phase.<sup>24,27,28</sup> The increase of charge density on the mineral surface will lead to a higher electric field that extends the hydration layer between the mineral surface and CO<sub>2</sub>.<sup>32</sup> Similarly, the role of ionic strength on double layer thickness is well established.<sup>17</sup> Increases in salinity compress the EDL, which can be quantified using the Debye-Hückel theory.<sup>33</sup>

Recent efforts to explore the mechanism controlling the thickness of the thin adsorbed water film separating a solid surface and CO<sub>2</sub> have relied on Hamaker and DLVO theories.<sup>17</sup> Pressure, temperature, ionic strength, and pH can be shown to modify the structure of the nanometer-scale water film by affecting the enclosed EDL interactions. pH is particularly interesting because the presence of high CO<sub>2</sub> partial pressures under GCS conditions will lead to low pH values (~3) in the

brine. But  $\text{CO}_2$ , a weak acid, does not alter the surface structure as dramatically as other contaminants typically found in flue gas (e.g., sulfur or nitrogen acids) would. These acids could also dramatically alter the charge balance at the mineral surface making it highly unlikely that a nonpolar molecule would be able to interact via weak van der Waals forces.<sup>17</sup>

Measuring these forces directly is difficult because of the elevated pressures that are involved.<sup>34</sup> Atomic force microscopy (AFM) is one of the most accurate tools for measuring adhesive forces and active research is underway to carry it out under supercritical  $\text{CO}_2$  conditions.<sup>35</sup> Studies of adhesion between solid surfaces have employed ‘stick-peel-crack’ type measurements where surfaces are placed in contact with each other and then pulled apart while measuring the force needed to separate the surfaces. Analogues exist in the context of wettability measurements on a polished mineral surface. The advancing and receding contact angle test in which a droplet is slowly introduced to the surface and then removed allows for the observation of many of the same phenomena. The effect of adhesion is seen most prominently during the receding portion of the experiment when work is done to overcome adhesive forces to separate surfaces that are originally in close contact. The adhesive forces that are counteracting the change in elastic potential energy as the droplet gets drawn away from the mineral interface are visible as the droplet is deformed.

Published work to date suggests that adhesion could be contributing to wettability hysteresis and contact line pinning in multiphase systems on mineral surfaces.<sup>9</sup> Few papers have explored adhesion processes explicitly and a more detailed understanding of the physicochemical conditions that contribute to adhesion is needed. The goal of this work is to test several hypotheses related to  $\text{CO}_2$  adhesion on the hydrated mineral interface. The first hypothesis is that brine chemistry, specifically ionic strength and pH, will have important, and potentially competing impacts on adhesion since they both influence the properties of the EDL at the surface. The second hypothesis is that mineral roughness will control the extent to which adhesion occurs on a smoother surface exhibiting considerably more adhesion than more rough surfaces.

## MATERIALS AND METHODS

Adhesion was studied under both equilibrium and dynamic conditions under reservoir pressure and temperature conditions ( $50^\circ\text{C}$  and  $20\text{ MPa}$ ) and a range of pH and ionic strength in fresh and carbonated synthetic brines on pendant droplets using methods previously reported by the authors.<sup>6</sup> By convention, all contact angle values here are reported in the aqueous phase. Seven representative minerals including quartz, calcite, amorphous silica, dolomite, kaolinite, illite, and phlogopite mica were selected since these constitute most of the minerals on the pore surfaces in sandstones.<sup>36</sup> These minerals all have hydroxyl functional groups, for example, aluminol ( $\equiv\text{Al}-\text{OH}$ ), silanol ( $\equiv\text{Si}-\text{OH}$ ), silanediols ( $=\text{Si}(\text{OH})_2$ ) and bridged hydroxyls ( $\equiv\text{Si}-\text{O}-\text{Si}\equiv$ ), at the solid surface and are sensitive to the adjacent aqueous phase pH and ionic strength conditions. Phlogopite mica was selected as a model mica species recognizing that many of the surface characteristics of interest in adhesion (e.g., surface functional groups, surface roughness) are shared by other mica species (i.e., muscovite and biotite).

Mineral samples were prepared by sectioning high purity rocks (Ward’s Natural Science), lapping the experimental surface according to the crystal structure with a diamond

grinding wheel, and then polishing them with a series of silicon carbide sanding papers down to a roughness of  $1\text{--}5\ \mu\text{m}$ . Some of the surfaces did not need polishing. Phlogopite cleaved easily into basal plane sheets to create surfaces that are smooth on the scale of 10 s of nanometers. The high-purity amorphous silica was not polished and used as received since it was polished at the factory (Heraeus Quarzglas). Some of the phlogopite and silica surfaces were made more rough using the sand papers in order to study the effect of roughness on adhesion. Roughness was measured using a profilometer (Dektak 8, Veeco) for the rough surfaces and an AFM (Asylum Research cypher scanning probe microscope) for smooth surfaces. Before experiments, all equipment and samples were carefully cleaned following the protocol previously described by the authors.<sup>6,37</sup> Extensive care was taken to exclude any source of contamination, especially organic matter which could strongly affect wettability. All samples were flushed with at least  $200\text{ mL}$  ( $\sim 10$  times pressure vessel volume) brine solution over 1 h to equilibrate the surfaces of the minerals with the aqueous phase. All experiments were repeated at least three times.

To evaluate adhesion of  $\text{CO}_2$  droplets on the mineral surface, a modified form of the advancing/receding contact angle measurement was carried out. To more closely approximate the mechanics of the ‘stick-peel-crack’ tests used to measure axial tensile force in solid mechanics, which is proportional to the adhesive energy and work of adhesion,<sup>14</sup> we positioned the injection needle  $1.5\text{--}3\text{ mm}$  below the surface and then outfitted the injection tubing with two pin valves. These two pin valves in sequence allowed for the precise control of captive  $\text{CO}_2$  droplet flows into and out of the pressure cell by regulating the relative pressure of the pure  $\text{CO}_2$  in the space between the valves and the pressure in the vessel.  $\text{N}_2$  control experiments were conducted under identical conditions on phlogopite and silica surfaces. Adhesion was determined based on the tendency of a  $\text{CO}_2$  droplet to stick to the mineral surface under tensile force created by the pressure difference between the injection needle and the pressure vessel. Irregular contact lines and increased wettability were also common qualitative characteristics of adhered droplets. More information about the experimental setup is available in the Supporting Information (SI).

## RESULTS AND DISCUSSION

Adhesion was observed for many of the  $\text{CO}_2$  droplets on phlogopite, amorphous silica, and calcite surfaces. When adhesion happened, the spontaneous ‘adhesive jumping’ of  $\text{CO}_2$  was observed, indicating dissipation of excess surface free energy.<sup>14</sup> The adhered droplets wetted the surface more fully and also became attached to the mineral in a way that made them difficult to remove. In contrast,  $\text{CO}_2$  droplets on quartz, dolomite, kaolinite, and illite surfaces did not wet the surface and exhibited contact angles ranging between  $16^\circ$  and  $22^\circ$ . Subtle changes to the contact angles of droplets that were not adhered could be induced by changing the solution chemistry as previously reported.<sup>6</sup> The difference between those droplets that exhibited adhesion and those that did not is shown in Figure 2. Droplets exhibiting no adhesion typically had a small contact with the mineral surface (Figure 2a). Adhered droplets (Figure 2b) were much more wetting (larger  $\Theta$ ) and there were often differences between the left and right side contact angle of the droplet suggesting that the triple phase line is not circular and distorted. This asymmetric character of adhered droplets has been reported as a consequence of pinning and by

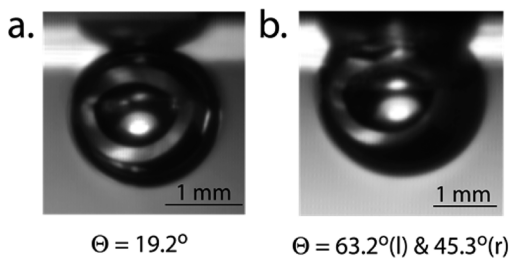


**Figure 2.** Droplet images reveal difference between a. droplets exhibiting no adhesion and b. droplets exhibiting adhesion on phlogopite ( $1.5\text{ M NaCl}$  ( $I = 1.20\text{ M}$ ) and  $P_{\text{CO}_2} = 0$ ). In b. the asymmetry between contact angles on left and right of the droplet are characteristic of contact line pinning (i.e., stationary contact lines as volume of droplets changes) and triple line distortion (i.e., noncircular contact between the droplet and the solid due to heterogeneities in the surface energy forces driving interfacial properties).

heterogeneities on the surface in terms of energy states and surface roughness. This contact line distortion resulting in irregular triple lines are uncommon for droplets that are nonwetting and not adhered to the surface like those in Figure 2a.

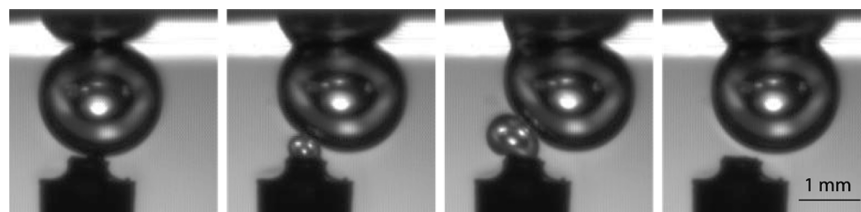
Adhesion force and wettability are not linearly correlated. Adhesion generally results in more wetting droplets but more wetting droplets do not necessarily result in adhesion. As mentioned earlier, wettability alteration and distorted three phase lines were used as a proxy for adhesion. The most dramatic manifestation of adhesion was the comparatively strong forces that bound the droplet to the mineral surface. Droplets that did not exhibit adhesion could move readily across the surface, like balls rolling across a table. Droplets that exhibited adhesion were highly resistant to shear forces in the brine (e.g., turbulent shear created using a stir bar), to tilting of the pressure vessel, and to the introduction of other droplets. Figure 3 shows how the creation of a new droplet, which would push a nonadhered droplet along the surface, instead lead to displacement and deformation of both by the adhered droplet. The contact between the droplet and the mineral surface increased. Eventually, the interfacial tension separating the droplets was overcome by the adhesive forces and the new droplet combined with the previous droplet at the surface. A theoretical description of the relationship between contact angle, interfacial tension, surface roughness, work of adhesion and adhesion force is provided in the SI.

Advancing and receding wettability tests were carried out as a means of understanding the dynamic effect that adhesion has on interfacial behavior including adhesion hysteresis and adhesion force. Figure 4 shows the progression, left to right,

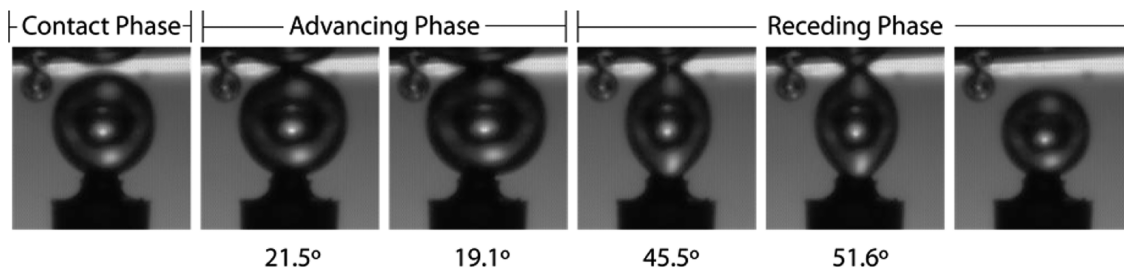
of a droplet being introduced to a phlogopite surface, contacted with the sample, expanded along the surface, then retracted back into the injection needle. The change in the contact angle is evident (and quantified at the bottom of the figure) as the droplet maintains contact with the mineral surface until the tensile forces act through the interfacial tension of the droplet overcome the adhesion forces and the droplet detaches. As a reference, the droplet on the left in each picture is not adhered to the surface. For droplets that do not adhere, advancing and receding experiments show negligible differences between advancing and receding contact angle and there is no distortion in the shape of the droplet. The tensile stress created during the receding phase induces deformation and enlarges the surface area of the  $\text{CO}_2$  droplet while interfacial tension acts to minimize the surface area. Snap-off can occur as a result of the competition between these two forces.

Figure 5 shows the results of a number of advancing and receding tests on both phlogopite (black lines) and silica (red lines) surfaces. Each line represents an individual test and the solid lines are for advancing contact angle while the dotted lines are for receding contact angles. The contact line length of these droplets are normalized in the  $x$ -axis to illustrate that this effect is observed for droplets over a range of sizes (droplet size ranging from 1.5 to 3.0 mm). In all cases, the advancing contact angles were highly consistent and changed very little as the droplet spread across the surface. The receding contact angles varied considerably as droplets adhered to the surface. In some cases, the receding contact angle value was 2–3 times higher than the advancing contact angle. For mineral surfaces in equilibrium with deionized water (Figure 5a), the adhesion effect and associated wettability hysteresis was modest but it increased with  $P_{\text{CO}_2}$  (Figure 5b), ionic strength (Figure 5c), or both (Figure 5d). For mineral samples that were in contact with strong acid (Figure 5e) or base (Figure 5f), negligible differences in advancing and receding contact angles were observed, indicating adhesion is highly sensitive to extremes in pH. Conceptually, solution pH will impact the surface charge density and balance, EDL structure and density of surface functional groups. All these factors likely influence the prevalence of adhesion.

The results in Figure 5 illustrate the nonlinear progression of receding contact lines. This behavior can be better understood in terms of a kinetic drag effect, namely adhesive drag.<sup>38</sup> Droplet detachment is retarded by the adhesion at the surface and as the droplet is pulled away from the surface, it will eventually yield, producing a step-like profile as observed in many of the curves in Figure 5. This is because time is required for local surface structures (i.e., surface functional groups and associated EDL) to evolve.<sup>14,38</sup> This effect can be quantified by



**Figure 3.** Droplets that adhere to the mineral surface can resist significant shear forces including those created here by introducing a droplet adjacent to the adhered droplet. In these time-lapse photos, the droplet is introduced in the second photo from the left. As it grows, the adhered droplet is displaced and eventually the new droplet combines with the existing droplet without removal of the adhered droplet (but increases in contact angle and in the contact length that corresponds to the greater volume of  $\text{CO}_2$  in the droplet). These experiments were conducted on phlogopite surface ( $1.5\text{ M NaCl}$  ( $I = 1.20\text{ M}$ ),  $P_{\text{CO}_2} = 0$ ).



**Figure 4.** Wettability hysteresis (advancing and receding) tests of a  $\text{CO}_2$  droplet exhibiting adhesion on a smooth phlogopite surface ( $1.5 \text{ M NaCl}$  ( $I = 1.21 \text{ M}$ ),  $P_{\text{CO}_2} = 20 \text{ MPa}$ ). The droplet was first introduced to the surface (far left) and the contact angle stayed approximately constant as  $\text{CO}_2$  was injected and the droplet advanced across the surface. As the droplet was drawn back into the injection needle, the adhesion forces deformed the droplet and altered the contact angle. Interfacial tension forces eventually overcome the adhesion force and the droplet broke away from the surface.

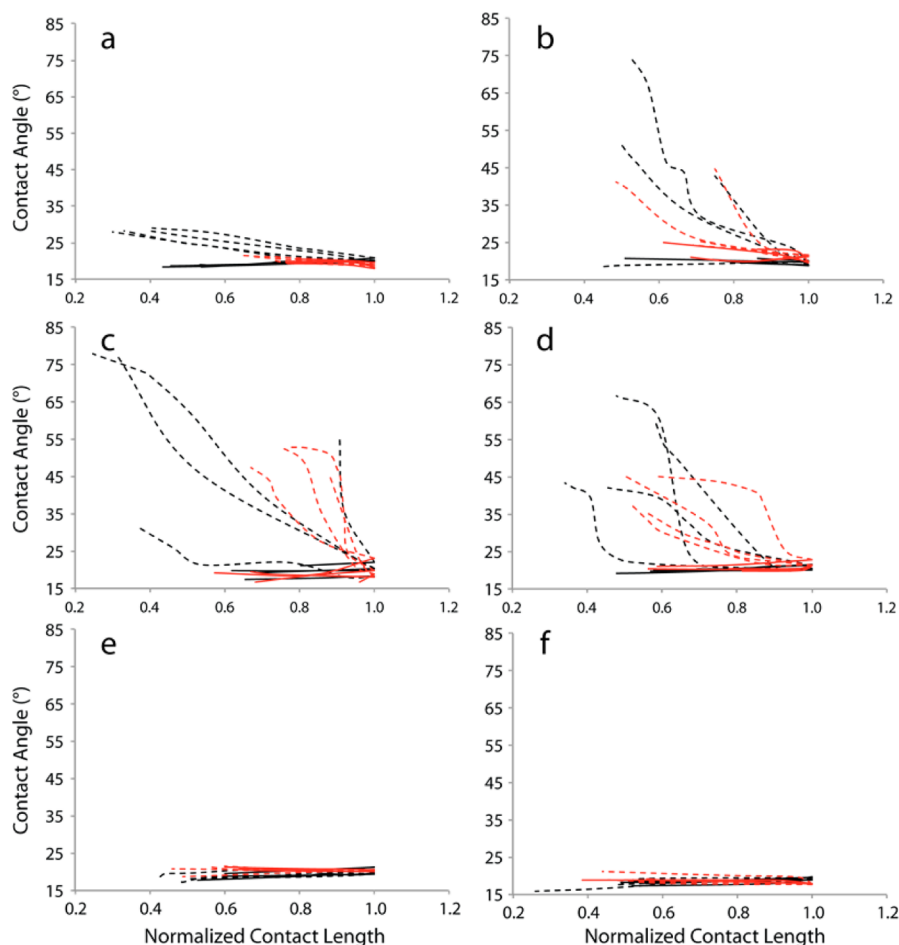


**Figure 5.** Contact angle hysteresis in advancing and receding tests show how adhesion can lead to enhanced wetting on the mineral surface as the droplet is stretched away from the surface. Phlogopite = black lines; Silica = red lines. Solid lines represent  $\text{CO}_2$  advancing contact angle and dotted lines are  $\text{CO}_2$  receding contact angles for a)  $I = 0$ ,  $P_{\text{CO}_2} = 0$ , pH 6.6; b)  $I = 10^{-3} \text{ M}$ ,  $P_{\text{CO}_2} = 20 \text{ MPa}$ , pH 2.9; c)  $I = 1.20 \text{ M}$  (1.5 M NaCl),  $P_{\text{CO}_2} = 0$ , pH 6.5; d)  $I = 1.21 \text{ M}$  (1.5 M NaCl),  $P_{\text{CO}_2} = 20 \text{ MPa}$ , pH 2.8; e)  $I = 1.22 \text{ M}$  (0.1 M HCl + 1.4 M NaCl),  $P_{\text{CO}_2} = 20 \text{ MPa}$ , pH 1.0; f)  $I = 1.24 \text{ M}$  (1.0 M NaOH + 0.5 M NaCl),  $P_{\text{CO}_2} = 20 \text{ MPa}$ , pH 5.5. Adhesion was highly reproducible on phlogopite and less consistent on silica where approximately one out of three replicates contained droplets exhibiting adhesion and these replicates had fewer adhered droplets than phlogopite. The data for silica surfaces that did not exhibit adhesion are not included here for clarity.

means of the adhesion (pull-off) force, work of adhesion and the interfacial thermodynamics. The extent of the adhesive drag has been reported to depend on the history of exposure of the surface, the duration that the surfaces have been in contact and the rate and magnitude of the peeling force applied. This behavior is consistent with theories about adhesive drag and hysteresis and provides another characterization of the strong adhesion forces acting at the surface.<sup>14</sup>

In spite of the striking contrast between droplets exhibiting adhesion and those that do not, the effect was not deterministic with respect to mineral surface and brine conditions. In other words, the frequency with which droplets adhered to the surface varied considerably even though the treatment of surfaces remained the same. For a phlogopite surface in DI water, only about 20% of the droplets adhered to the surface. When the phlogopite surface was equilibrated with brine

instead of DI water, the percentage of droplets that adhered increased to >50% of the droplets. These trends were statistically significant and observed over multiple replicates and thousands of droplets. The addition of salt or CO<sub>2</sub> increased the incidence of adhesion considerably, indicating that brine chemistry was important in controlling adhesion. A clear increase in the prevalence of adhesion as a function of ionic strength is shown in Table 1. The results in Table 1 also

**Table 1.** Incidence of Adhesion on Smooth and Chemically Homogenous Surfaces Was Impacted by Several Factors Including Ionic Strength and P<sub>CO<sub>2</sub></sub><sup>a</sup>

phlogopite and CO <sub>2</sub>		
P <sub>CO<sub>2</sub></sub> (MPa)	0	20
ionic strength (M)	droplets adhered (%)	
0.00	26 ± 13	19 ± 11
0.10	49 ± 14	82 ± 17
0.46	58 ± 25	76 ± 13
0.86	52 ± 17	71 ± 23
1.21	55 ± 12	79 ± 7
silica and CO <sub>2</sub>		
P <sub>CO<sub>2</sub></sub> (MPa)	0	20
ionic Strength (M)	droplets adhered (%)	
0.00	9 ± 16	26 ± 44
1.21	38 ± 49	31 ± 54
phlogopite and N <sub>2</sub>		
P <sub>N<sub>2</sub></sub> (MPa)	0	20
ionic strength (M)	droplets adhered (%)	
0.00	24 ± 15	30 ± 22
1.21	35 ± 20	23 ± 12
silica and N <sub>2</sub>		
P <sub>N<sub>2</sub></sub> (MPa)	0	20
ionic strength (M)	droplets adhered (%)	
0.00	74 ± 46	66 ± 53
1.21	66 ± 54	67 ± 55

<sup>a</sup>The prevalence of carbonate ions and salt in the solution increased the incidence of adhesion. The effect of pressure was attributed to the influence of increased carbonate ions in solution since analogous experiments carried out using nitrogen showed no effect from pressure. Error range represents one standard deviation and is meant to indicate the large variation between replicates. It should be noted that negative percentage is not realistic.

reveal the relationship between P<sub>CO<sub>2</sub></sub> and adhesion. In all cases, the presence of dissolved CO<sub>2</sub> in the brine increased the proportion of droplets adhered to the mineral surface.

It is important to emphasize that the confidence interval on these data was large, even though each experiment was repeated multiple times primarily because of heterogeneities in actual rock composition and structure at the molecular level and ways in which this surface was impacted by solution chemistry. Even though the trends reported here are robust for the conditions under which we tested them, we made every effort not to generalize trends beyond what the confidence intervals suggest. Conceptually, the challenge of repeatability in these experiments can be attributed to the fact that distribution and density of different surface groups (e.g., silanol ( $\equiv\text{Si}-\text{OH}$ ) or silanediols ( $=\text{Si}(\text{OH})_2$ )) can impact general and local wettability characteristics. Hydroxylation, dehydration, dehy-

droxylation, and rehydroxylation all impact the wettability of a mineral sample.<sup>22</sup>

To further explore the effect of pressure, experiments were carried out using pressurized N<sub>2</sub> instead of CO<sub>2</sub>. These results are also shown in Table 1. On both phlogopite and silica surfaces, adhesion was prevalent, though more so on silica than on phlogopite, unlike the CO<sub>2</sub> experiments. The average contact angle for N<sub>2</sub> on silica was higher than the contact angle for any other case tested here. Increased N<sub>2</sub> partial pressure had no statistically independent effect on adhesion. This makes sense because our hypothesis was that the increase in CO<sub>2</sub> partial pressure increased the concentration of carbonate and bicarbonate ions, which substituted the hydrogen in the hydroxyl groups and excluded water molecules from interacting with the hydroxyl groups due to the “umbrella effect” described by Wang et al. and Gao et al. effectively enhancing the adhesion effect.<sup>18,39</sup> In the N<sub>2</sub> experiments, the presence of strong acid and base also eliminated the prevalence of adhesion on the mineral surface. Both CO<sub>2</sub> and N<sub>2</sub> would be expected to preferentially adhere to mineral surfaces with the lowest net charge. To ensure that no organic residuals were interfering with the results collected here, the vessel was filled with acetone instead of brine and the experiments were repeated. No significant increase in incidence of adhesion was observed.

Adhesion was most readily observed on phlogopite and silica surfaces initially (as shown in Figure 5 and supported in Table 1) because these were the most smooth surfaces initially tested here. The fused amorphous silica was received as a highly polished surface of high purity and the phlogopite could be cleaved to form virtually atomically smooth sheets without the need for polishing. The samples of quartz, calcite, dolomite, kaolinite, and Illite were prepared using polishing techniques described in the Materials and Methods section. The calcite could also be cleaved along the rhombohedral plane to achieve highly smooth surfaces, even though some crystal steps were still evident perpendicular to the cleavage.

To better characterize the effect of surface roughness on adhesion, additional experiments were carried out for phlogopite, calcite, and amorphous silica where the roughness of the surface was intentionally controlled. Both smooth mineral surfaces (on the scale of nanometers) and rougher surfaces (polished to micrometer smoothness) were prepared as shown in Table 2. The results show a clear drop in the incidence of adhesion with increased roughness. This effect could not be overcome by higher partial pressures of CO<sub>2</sub>. It supports previously reported observations of adhesion only on mica surfaces since these are the easiest to cleave into

**Table 2.** Surface Roughness Has an Important Effect on the Prevalence of Adhesion (1.5 M NaCl (I = 1.21 M), P<sub>CO<sub>2</sub></sub> = 20 MPa)

mineral	roughness (nm)	P <sub>CO<sub>2</sub></sub> (MPa)	
		0	20
phlogopite	6.4 ± 1.0	55 ± 12	79 ± 7
	1600 ± 472	4 ± 6	11 ± 13
calcite	1.9 ± 1.4	8 ± 4	6 ± 6
	4725 ± 1195	2 ± 1	1 ± 1
amorphous silica	5.8 ± 1.8	38 ± 49	31 ± 54
	2300 ± 360	1 ± 1	1 ± 0

nanometer-smooth surfaces. Adhesion has been explained in terms of molecular forces that act on the nanometer scale and these results support this explanation.<sup>14</sup> In contrast, calcite exhibited little adhesion of CO<sub>2</sub> and N<sub>2</sub> at either roughness, but there is significant dissolution at the calcite surface, which may interfere with the development of adhesion – a characteristic that has been reported before in carbonate-rich caprock.<sup>40</sup> It should be noted that even though initial roughness was controlled on calcite surfaces, dissolution reactions led to changes in surface smoothness over the course of an experiment.

The surface roughness effect can be understood in part on the basis of the size of the CO<sub>2</sub> droplet with smaller CO<sub>2</sub> droplets being preferentially adhesive. The relationship between adhesive force and gravitational force provides good estimates of the critical droplet size of adhesion and it is affected by the surface roughness and it will help to begin assessing the implications of this adhesion in porous media where pore size will limit the size of CO<sub>2</sub> droplets.

A final observation from these experiments was that adhesion was not a perfectly reversible process. After adhesion was observed in fresh DI water, the pressure vessel was vented and flushed with ~5 times vessel volumes of fresh DI water. Once pressure and temperature recovered to the original conditions, supercritical CO<sub>2</sub> droplets were reintroduced to the phlogopite surface. No adhesion occurred even when all the other process variables stayed the same, indicating that the conditions at the phlogopite surface (e.g., the charge and density of the surface hydroxyl groups, the thickness of the EDL, etc.) had changed. After the system had reached equilibrium over the course of several hours, the phlogopite surface began to exhibit adhesion with CO<sub>2</sub> again. The exact kinetics of these processes, particularly in light of the time scales that are relevant for GCS, were not fully characterized here. Over time, droplets would adhere to the surface again because it is an energetically favorable process. A triggering source, such as a pressure gradient or shear force in the pressure cell, may be necessary to initiate adhesion.

## ■ ENVIRONMENTAL IMPLICATIONS

Adhesion could have important implications for multiphase flow through porous media in the context of GCS. It could increase the residual trapping capacity of porous media due to the wettability alteration (e.g., more CO<sub>2</sub>-philic) and added immobility from adhesion. Past work suggests that CO<sub>2</sub>(g) will exhibit more adhesion than CO<sub>2</sub>(l) or CO<sub>2</sub>(sc) further supporting the notion that adhesion could be an important process in controlling CO<sub>2</sub> leakage from target formations.<sup>9</sup> On reactive surfaces, like phlogopite and calcite, the intimate contact between CO<sub>2</sub> and the mineral surface could lead to enhanced reaction kinetics.<sup>41</sup> The results obtained here point to the importance of understanding the chemistry of connate brines and the composition and morphology of diagenetic minerals on the pore wall for predicting when adhesion will occur.

## ■ ASSOCIATED CONTENT

### Supporting Information

More information about our experimental methods and additional results are available online at <http://pubs.acs.org>. This material is available free of charge via the Internet at <http://pubs.acs.org>.

## ■ AUTHOR INFORMATION

### Corresponding Author

\*(A.F.C.) Phone: 1-434-924-7966; fax: 1-434-982-2951; e-mail: aclarens@virginia.edu.

### Notes

The authors declare no competing financial interest.

## ■ ACKNOWLEDGMENTS

We thank Yonghang Pei and Keye Sun for their assistance in AFM and profilometer data collection and interpretation as well as James Danberg for sample preparation. This work was funded by the National Science Foundation (Grant No. CBET-1134397).

## ■ REFERENCES

- (1) Jun, Y. S.; Giammar, D. E.; Werth, C. J. Impacts of geochemical reactions on geologic carbon sequestration. *Environ. Sci. Technol.* **2013**, *47* (1), 3–8, DOI: 10.1021/es3027133.
- (2) Chiquet, P.; Broseta, D.; Thibeau, S. Wettability alteration of caprock minerals by carbon dioxide. *Geofluids*. **2007**, *7* (2), 112–122, DOI: 10.1111/j.1468-8123.2007.00168.x.
- (3) Morrow, N. R.; Tang, G.-q.; Valat, M.; Xie, X. Prospects of improved oil recovery related to wettability and brine composition. *J. Pet. Sci. Eng.* **1998**, *20* (3–4), 267–276, DOI: 10.1016/s0920-4105(98)00030-8.
- (4) Chalbaud, C.; Robin, M.; Bekri, S.; Eggermann, P. In *Wettability Impact on CO<sub>2</sub> Storage in Aquifers: Visualisation and Quantification Using Micromodel Tests, Pore Network Model and Reservoir Simulations*; International Symposium of the Society of Core Analysts: Calgary, Canada, 2007.
- (5) Mills, J.; Riazi, M.; Sohrabi, M. Wettability on common rock-forming minerals in a CO<sub>2</sub>-brine system at reservoir conditions. In *International Symposium of the Society of Core Analysts*, Austin, TX 18–21 September, 2011.
- (6) Wang, S.; Edwards, I.; Clarens, A. F. Wettability phenomena at the CO<sub>2</sub>-brine-mineral interface: Implications for geologic carbon sequestration. *Environ. Sci. Technol.* **2013**, *47* (1), 234–241, DOI: 10.1021/es301297z.
- (7) Mansoori, S. A.; Iglauer, S.; Pentland, C. H.; Bijeljic, B.; Blunt, M. J. Measurements of non-wetting phase trapping applied to carbon dioxide storage. *Energy Procedia* **2009**, *1* (1), 3173–3180, DOI: 10.1016/j.ijggc.2009.09.013.
- (8) Bikkina, P. K. Contact angle measurements of CO<sub>2</sub>-water-quartz/calcite systems in the perspective of carbon sequestration. *Int. J. Greenhouse Gas Control* **2011**, *5* (5), 1259–1271, DOI: 10.1016/j.ijggc.2011.07.001.
- (9) Broseta, D.; Tonnet, N.; Shah, V. Are rocks still water-wet in the presence of dense CO<sub>2</sub> or H<sub>2</sub>S? *Geofluids*. **2012**, DOI: 10.1111/j.1468-8123.2012.00369.x.
- (10) Carre, A.; Lacarriere, V. Study of surface charge properties of minerals and surface-modified substrates by wettability measurements. *Contact Angle, Wettability Adhes.* **2006**, *4*, 1–14.
- (11) Hong, S.-J.; Chang, F.-M.; Chou, T.-H.; Chan, S. H.; Sheng, Y.-J.; Tsao, H.-K. Anomalous contact angle hysteresis of a captive bubble: Advancing contact line pinning. *Langmuir*. **2011**, *27* (11), 6890–6896, DOI: 10.1021/la2009418.
- (12) Juanes, R.; Spiteri, E. J.; Orr, F. M., Jr.; Blunt, M. J. Impact of relative permeability hysteresis on geological CO<sub>2</sub> storage. *Water Resour. Res.* **2006**, *42* (12), W12418 DOI: 10.1029/2005WR004806.
- (13) Shah, V.; Broseta, D.; Mouronval, G. C. In *Capillary Alteration of Caprocks by Acid Gases*, SPE/DOE Symposium on Improved Oil Recovery, 2008.
- (14) Kendall, K. Adhesion: Molecules and mechanics. *Science*. **1994**, *263*, 1720–1725, DOI: 10.1126/science.263.5154.1720.
- (15) Dzyaloshinskii, I.; Lifshitz, E.; Pitaevskii, L. P. General theory of van der Waals' Forces. *Phys.-Usp.* **1961**, *4* (2), 153–176.

- (16) Gordesli, F. P.; Abu-Lail, N. I. Combined poisson and soft-particle DLVO analysis of the specific and nonspecific adhesion forces measured between l. monocytogenes grown at various temperatures and silicon nitride. *Environ. Sci. Technol.* **2012**, *46* (18), 10089–10098.
- (17) Tokunaga, T. K. DLVO-based estimates of adsorbed water film thicknesses in geologic CO<sub>2</sub> reservoirs. *Langmuir*. **2012**, *28* (21), 8001–8009, DOI: 10.1021/la2044587.
- (18) Wang, M.; Chen, C.; Ma, J.; Xu, J. Preparation of superhydrophobic cauliflower-like silica nanospheres with tunable water adhesion. *J. Mater. Chem.* **2011**, *21* (19), 6962–6967, DOI: 10.1039/C1JM10283D.
- (19) Jung, J.; Wan, J. Wettability alteration upon reaction with scCO<sub>2</sub>: Silica, mica, and calciteIn *American Geophysical Union - Fall Meeting*, San Francisco, CA, 2011.
- (20) Buckley, J. S.; Takamura, K.; Morrow, N. R. Influence of electrical surface charges on the wetting properties of crude oils. *SPE Reservoir Eng.* **1989**, August, 332–340.
- (21) Carroll, S. A.; Maxwell, R. S.; Bourcier, W.; Martin, S.; Hulsey, S., Evaluation of silica-water surface chemistry using NMR spectroscopy. *Geochim. Cosmochim. Acta* **2002**, *66*, (6), 913–926; DOI: 10.1016/S0016-7037(01)00827-4.
- (22) Zhuravlev, L. T. The surface chemistry of amorphous silica. Zhuravlev model. *Colloids Surf., A* **2000**, *173* (1), 1–38, DOI: 10.1016/S0927-7757(00)00556-2.
- (23) McCool, B.; Tripp, C. P. Inaccessible hydroxyl groups on silica are accessible in supercritical CO<sub>2</sub>. *J. Phys. Chem. B* **2005**, *109* (18), 8914–8919, DOI: 10.1021/jp050192q.
- (24) Tripp, C. P.; Combes, J. R. Chemical modification of metal oxide surfaces in supercritical CO<sub>2</sub>: The interaction of supercritical CO<sub>2</sub> with the adsorbed water layer and the surface hydroxyl groups of a silica surface. *Langmuir*. **1998**, *14* (26), 7348–7352, DOI: 10.1021/la9805701.
- (25) Cole, D. R.; Chialvo, A. A.; Rother, G.; Vlcek, L.; Cummings, P. T. Supercritical fluid behavior at nanoscale interfaces: Implications for CO<sub>2</sub> sequestration in geologic formations. *Philos. Mag.* **2010**, *90* (17–18), 2339–2363, DOI: 10.1080/14786430903559458.
- (26) Vishnyakov, A.; Shen, Y.; Tomassone, M. S. Interactions of silica nanoparticles in supercritical carbon dioxide. *J. Chem. Phys.* **2008**, *129*, 174704, DOI: 10.1063/1.2994714.
- (27) Drelich, J.; Miller, J. D.; Good, R. J. The effect of drop (bubble) size on advancing and receding contact angles for heterogeneous and rough solid surfaces as observed with sessile-drop and captive-bubble techniques. *J. Colloid Interface Sci.* **1996**, *179* (1), 37–50, DOI: 10.1006/jcis.1996.0186.
- (28) Long, J.; Hyder, M.; Huang, R.; Chen, P. Thermodynamic modeling of contact angles on rough, heterogeneous surfaces. *Adv. Colloid Interface Sci.* **2005**, *118* (1–3), 173–190, DOI: 10.1016/j.cis.2005.07.004.
- (29) Nosonovsky, M. Model for solid-liquid and solid-solid friction of rough surfaces with adhesion hysteresis. *J. Chem. Phys.* **2007**, *126*, 224701, DOI: 10.1063/1.2739525.
- (30) Giljean, S.; Bigerelle, M.; Anselme, K.; Haidara, H. New insights on contact angle/roughness dependence on high surface energy materials. *Appl. Surf. Sci.* **2011**, *257*, 9631–9638, DOI: 10.1016/j.apsusc.2011.06.088.
- (31) Kerisit, S.; Cooke, D. J.; Spagnoli, D.; Parker, S. C. Molecular dynamics simulations of the interactions between water and inorganic solids. *J. Mater. Chem.* **2005**, *15* (14), 1454–1462, DOI: 10.1039/B415633C.
- (32) Yeganeh, M. S.; Dougal, S. M.; Pink, H. S. Vibrational spectroscopy of water at liquid/solid interfaces: Crossing the isoelectric point of a solid surface. *Phys. Rev. Lett.* **1999**, *83* (6), 1179–1182, DOI: 10.1103/PhysRevLett.83.1179.
- (33) Papirer, E. *Adsorption on Silica Surfaces*; CRC Press: Boca Raton, FL, 2000.
- (34) Lea, A. S.; Higgins, S. R.; Knauss, K. G.; Rosso, K. M. A high-pressure atomic force microscope for imaging in supercritical carbon dioxide. *Rev. Sci. Instrum.* **2011**, *82* (4), 043709–043709–7, DOI: 10.1063/1.3580603.
- (35) Aradhya, S. V.; Frei, M.; Hybertsen, M. S.; Venkataraman, L. Van der Waals interactions at metal/organic interfaces at the single-molecule level. *Nat. Mater.* **2012**, *11*, 872–876.
- (36) Peters, C. A. Accessibilities of reactive minerals in consolidated sedimentary rock: An imaging study of three sandstones. *Chem. Geol.* **2009**, *265* (1–2), 198–208, DOI: 10.1016/j.chemgeo.2008.11.014.
- (37) Wang, S.; Clarens, A. F., The effects of CO<sub>2</sub>-brine rheology on leakage processes in geologic carbon sequestration. *Water Resour. Res.* **2012**, *48*, (8), W08518
- (38) Kendall, K. Peel adhesion of solid films-The surface and bulk effects. *J. Adhes.* **1973**, *5* (3), 179–202.
- (39) Gao, L.; McCarthy, T. J. Contact angle hysteresis explained. *Langmuir*. **2006**, *22* (14), 6234–6237.
- (40) Tonnet, N.; Broseta, D.; Mouronval, G. C. Evaluation of petrophysical properties of a carbonate-rich caprock for CO<sub>2</sub> geological storage purposes. In *SPE EUROPEC/EAGE Annual Conference and Exhibition*, Barcelona, Spain, 14–17 June, 2010.
- (41) Shao, H.; Ray, J. R.; Jun, Y.-S. Effects of salinity and the extent of water on supercritical CO<sub>2</sub>-induced phlogopite dissolution and secondary mineral formation. *Environ. Sci. Technol.* **2011**, *45* (4), 1737–1743, DOI: 10.1021/es1034975.

Supporting information for:

## **CO<sub>2</sub> adhesion on hydrated mineral surfaces**

Shibo Wang, Zhiyuan Tao, Sara M. Persily, Andres F. Clarens  
Civil and Environmental Engineering  
University of Virginia, Charlottesville, VA, 22904

Environmental Science and Technology

8 pages

### List of Figures

Figure S1 - Experimental setup .....	2
Figure S2 - AFM images of smooth mineral surfaces.....	4
Figure S3 - Surface roughness measurement for smooth amorphous silica.....	5
Figure S4 - Surface roughness measurement for smooth phlogopite ...	6
Figure S5 - Surface roughness measurement for smooth calcite .....	7

### List of Tables

Table S1 - Surface roughness of smooth silica .....	5
Table S2 - Surface roughness of smooth phlogopite.....	6
Table S3 - Surface roughness of smooth calcite .....	7
Table S4 – Profilometer measurements of rough mineral surfaces.....	8
Table S5 – Surface measurements summary .....	8

## **1 Experimental setup**

All experiments were carried out in a custom-built pressure vessel using the test rig shown in schematic form in Figure S1. The entire assembly is described in previous work by the authors [1]. Buoyant forces required the use of the pendant droplet method to measure the CO<sub>2</sub>-brine-mineral contact angle. To characterize wettability hysteresis, the captive droplet method was used where a CO<sub>2</sub> droplet was introduced to, or withdrawn from, a mineral sample surface from below. The needle extended up into the vessel such that the tip was 1.5-3 mm from the surface to enable the advancing/receding tests to be carried out. The mineral sample was fixed in place using a PTFE Teflon stage and the entire pressure vessel was positioned on a stability table to ensure that the bubble would be stationary during the measurements.

Two valves were positioned downstream of the vessel outlet to accurately add/withdraw small amounts of CO<sub>2</sub> to/from the CO<sub>2</sub> droplets inside the vessel

during the wettability hysteresis (advancing and receding) test. Stainless steel tubing (High Pressure Equipment Company) with an ID of 0.76 mm was positioned between the two valves and the length of tubing was adjusted based on the desired pressure gradient for given P/T conditions in the vessel . The two-valve control system was found to be the best technique to effectively control CO<sub>2</sub> droplet size and rate of change. It was not unlike a 6-way injection valve that is commonly used in chromatography applications. In this context, small pressure gradients (< 10 psi) could be achieved repeatably by properly adjusting these two valves. The results were even more accurate than those achieved using the syringe pump, alone which has a high precision pressure control function.

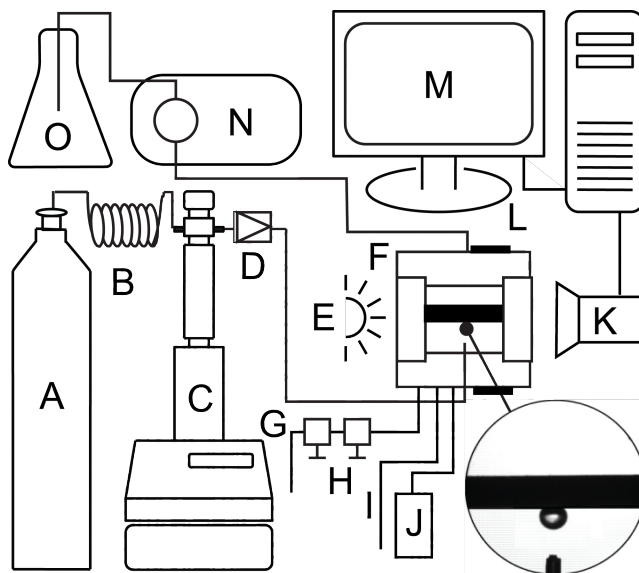


**Figure S1 - Experimental setup**

A – tank of food grade CO<sub>2</sub>, B – heat exchanger, C – syringe pump, D – one way valve, E – light source with diffuser, F – custom-built stainless steel 316 pressure vessel with sapphire windows, G – outlet, H – two pin valves for droplet control, I – thermocouple, J – pressure transducer, K – digital camera, L – heating tape, M – computer with DAQ, N – HPLC pump, O – brine.

## 2 Contact angle measurements

There are a variety of methods that have been developed to quantify contact angle based on images of droplets at the surface. Many have used the Axisymmetric Drop Shape Analysis (ADSA) method. The ADSA method is the most common technique for determining contact angle due to its precise match with the droplet shape and accurate reading of angles. A major limitation of the ADSA method is that it requires that droplets are symmetrical. In practice, droplets are often not symmetrical because of roughness, heterogeneity, contamination, adhesion and hysteresis. Another limitation of the ADSA method is that contact angles are determined by drawing tangential lines from the two ternary-phase contact points along the CO<sub>2</sub>-brine interface and this can

lead to significant errors based on image quality. To address this, the two ternary-phase contact points must be chosen very carefully and precisely.

To overcome these limitations, the Dropsnake algorithm has been developed and it applies to droplets of any shape. The contour of the droplet is defined using an image processing algorithm in the ImageJ software package and this is then confirmed by the user. The combined manual and automatic determination of contact angle requires considerably more time and effort but insured the most accurate representation of the data. This approach resolves the symmetry and contact point misplacement limitations of the ADSA methods. All the images containing the measuring line were carefully compared with the original image side by side to minimize error. Our experimental results were highly reproducible and were not influenced by the user carrying out the data analysis. Drop image analysis followed the same procedures described in our previous work [1].

### 3 Surface roughness characterization

The smooth silica sample was obtained from Heraeus Quarzglas and were highly polished and high purity intended for microscopy applications. All other mineral samples were obtained from Ward's Natural Science. Phlogopite was cleaved into sheets along the basal plane using a razor. Calcite samples were also split using a razor to create smooth crystal surfaces. All other minerals were processed using sand paper obtained from 3M. The sand paper has a roughness rating of P60 (average particle diameter is 269 $\mu\text{m}$ ).

#### 3.1 Roughness measurements - smooth surfaces

For mineral surfaces with surface roughness <1000 nm, atomic force microscopy was used to evaluate the surface roughness. The AFM was operated on amplitude mode on samples tested under ambient laboratory conditions in tapping mode. The probe is made of silica and is 160  $\mu\text{m}$  long with a radius of 9 nm. The tapping vibration mode limited the roughness of samples that could be measured using the AFM to  $\sim$ 100 nm. The scan area was 10  $\mu\text{m}$  by 10  $\mu\text{m}$ . Gwyddion® software is used to analyze the images. The amplitude retrace images of the smooth surfaces are shown in Figure S2. For each image, we measured the roughness at different locations in the field of view, e.g., top left to top right, middle left to middle right, bottom left to bottom right, top left to bottom left, top middle to bottom middle, top right to bottom right, top left to bottom right, bottom left to top right. An average surface roughness value was calculated along with standard deviation of the data.

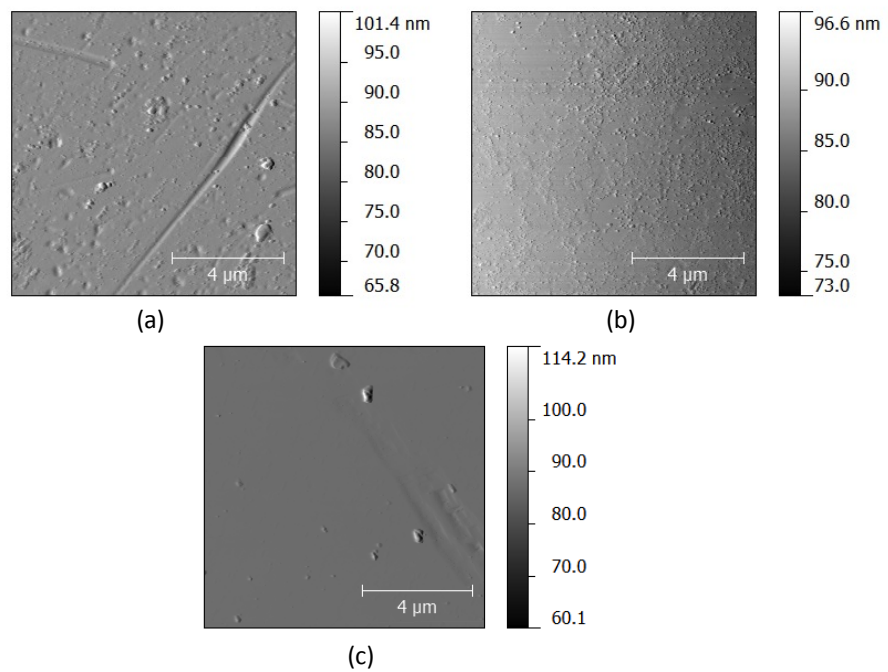


**Figure S2 - AFM images of smooth mineral surfaces.**

(a) Amorphous silica (b) Phlogopite (c) Calcite.

The results for smooth amorphous silica are shown in Figure S3 and Table S1. The surface roughness value for smooth amorphous silica is  $5.8 \pm 1.8$  nm.

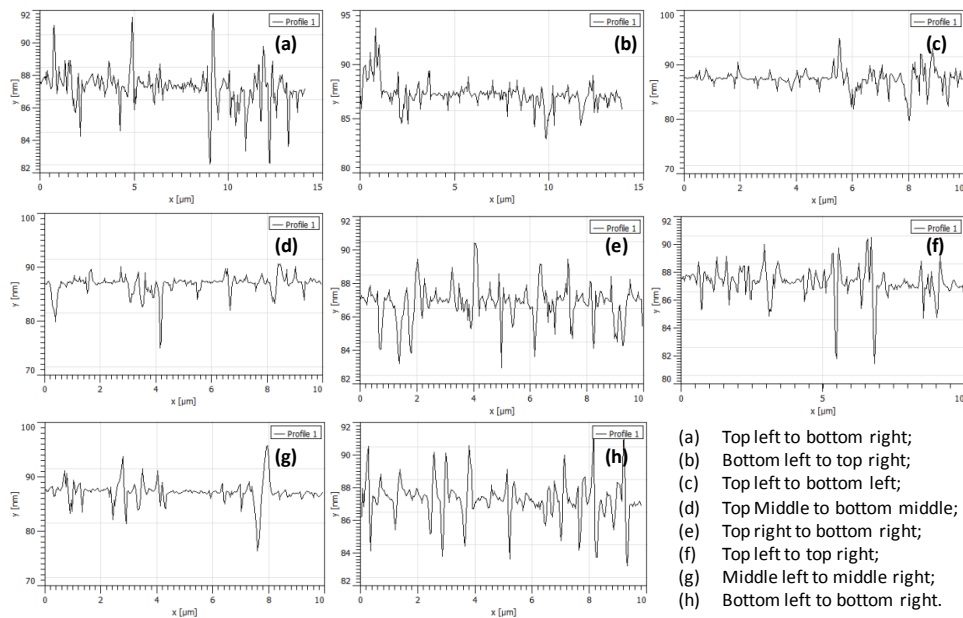


**Figure S3 - Surface roughness measurement for smooth amorphous silica.**

**Table S1 - Surface roughness of smooth silica**

Sample	Highest value (nm)	Lowest value (nm)	Average (nm)	Height (nm)
(a)	92	82.2	87.1	4.9
(b)	93.5	83.5	88.5	5
(c)	95.0	80.0	87.5	7.5
(d)	95	80	87.5	6.75
(e)	90.4	83	86.7	3.7
(f)	90.2	81.6	85.9	4.3
(g)	95	77	86	9
(h)	91.6	81.4	86.5	5.1

The results for smooth phlogopite are shown in Figure S4 and Table S4. Phlogopite had an average surface roughness of  $6.4 \pm 1.0$  nm.

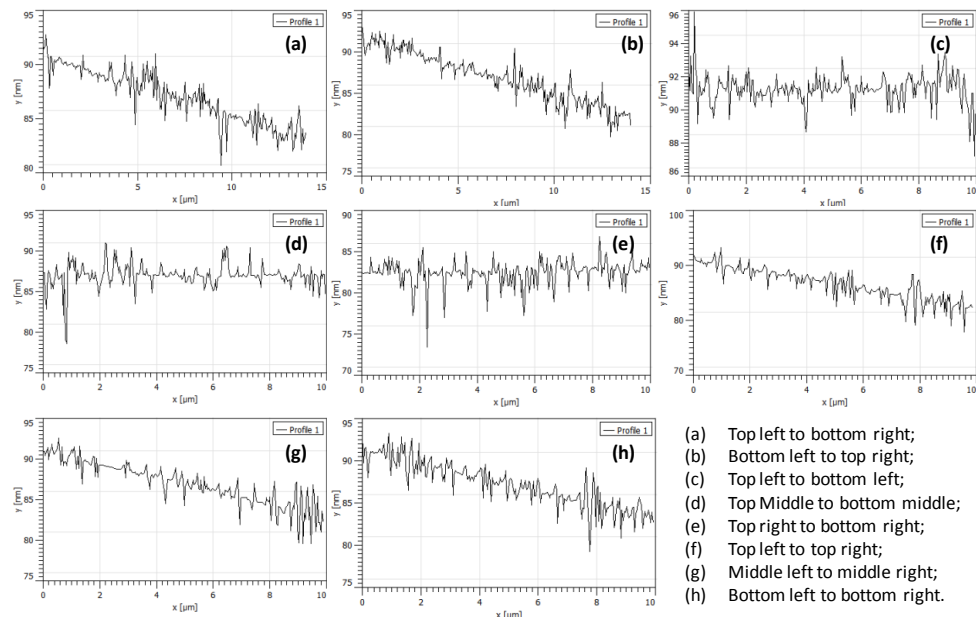
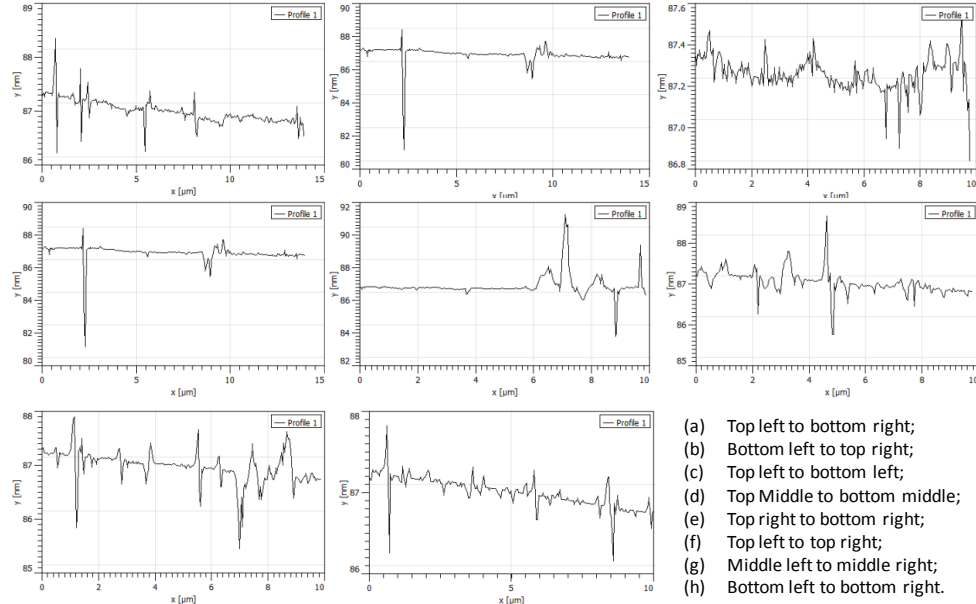


**Figure S4 - Surface roughness measurement for smooth phlogopite**

**Table S2 - Surface roughness of smooth phlogopite**

Sample	Highest value (nm)	Lowest value (nm)	Average (nm)	Height (nm)
(a)	92.5	80	86.2	6.25
(b)	93	80	86.5	6.5
(c)	96	87.6	91.8	4.2
(d)	91	78	84.5	6.5
(e)	87	74	80.5	6.5
(f)	93	78	85.5	7.5
(g)	93	79	86	7.0
(h)	93	79	86	7.0

The surface roughness measurement for smooth calcite are shown in Figure S5 and Table S3. The results for smooth calcite are  $1.9 \pm 1.4$  nm.



- (a) Top left to bottom right;
- (b) Bottom left to top right;
- (c) Top left to bottom left;
- (d) Top Middle to bottom middle;
- (e) Top right to bottom right;
- (f) Top left to top right;
- (g) Middle left to middle right;
- (h) Bottom left to bottom right.

**Figure S5 - Surface roughness measurement for smooth calcite**

**Table S3 - Surface roughness of smooth calcite**

Sample	Highest value (nm)	Lowest value (nm)	Average (nm)	Height (nm)
(a)	88.3	86.2	87.2	1.0
(b)	88.4	81.2	84.8	3.6
(c)	87.5	86.8	87.2	0.4
(d)	88.4	81.6	85	3.4
(e)	91.2	83.8	87.5	3.7
(f)	88.6	85.8	87.2	1.4
(g)	87.8	85.5	86.6	1.2
(h)	87.9	86.3	87.1	0.8

### 3.2 Roughness measurements - rough surfaces

The rough surfaces were measured using a profilometer (Dektak 8, Veeco). The measurement length was 5 mm. Each sample was measured several times at

different locations on the sample surface. An average surface roughness is reported with standard deviation. The results are reported in Tables S4.

**Table S4 – Profilometer measurements of rough mineral surfaces**

Sample	Measurements (nm)	Average (nm)
Rough Amorphous Silica	2200	$2300 \pm 360$
	2000	
	2700	
Rough Phlogopite	2200	$1600 \pm 472$
	1500	
	1300	
Rough Calcite	3900	$4725 \pm 1195$
	6500	
	4300	
	4200	

A summary of all the surface roughness measurements is presented in Table S5.

**Table S5 – Surface measurements summary**

Sample	Surface Roughness (nm)
Smooth Amorphous Silica	$5.8 \pm 1.8$
Rough Amorphous Silica	$2300 \pm 360$
Smooth Phlogopite	$6.4 \pm 1.0$
Rough Phlogopite	$1600 \pm 472$
Smooth Calcite	$1.9 \pm 1.4$
Rough Calcite	$4725 \pm 1195$

## 4 Video

To better illustrate some of the characteristic processes driving the interfacial adhesion results reported here, five videos are included in this supporting information document. They include videos on: (#1) CO<sub>2</sub> adhesion hysteresis, (#2-4) Strength of adhesion and (#5) CO<sub>2</sub> droplet snap-off due to interfacial tension.

## 5 Adhesion theory

Contact angle, interfacial tension and adhesion are interrelated and this section illustrates their connection. Most analyses of contact angle begin with Young's equation (Eq. S1), which relates contact angle to the interfacial forces between the three phases present in the system:

$$\gamma_{CO_2-Mineral} = \gamma_{CO_2-Brine} \cos\theta + \gamma_{Brine-Mineral} \quad \text{Eq. S1}$$

where  $\theta$  is the equilibrium contact angle and  $\gamma_{CO_2-Mineral}$ ,  $\gamma_{CO_2-Brine}$  and  $\gamma_{Brine-Mineral}$  are the three interfacial tension forces between  $CO_2$ , brine and mineral, respectively. Contact angle is often measured experimentally as it was in this work, but it can also be calculated from thermodynamic first principles (e.g., DLVO) as shown in Eq. S2 [2]:

$$\cos\theta = 1 + \frac{1}{\gamma_{CO_2-Brine}} \left[ \frac{A_{CO_2-Brine-Mineral}}{12\pi h_0^2} - \frac{\epsilon_0 (\psi_1 - \psi_2)^2}{8\pi h_0} + K\lambda e^{-\frac{h_0}{\lambda}} \right] \quad \text{Eq. S2}$$

where  $A_{CO_2-Brine-Mineral}$  is the  $CO_2$ -brine-mineral three phase Hamaker constant,  $h_0$  is the thickness of the water film at equilibrium,  $K$  and  $\lambda$  are the parameters of the structural forces,  $\epsilon_0$  is the dielectric constant of brine, and  $\psi_1$  and  $\psi_2$  are the potentials of the film-mineral and film- $CO_2$  interfaces. If contact angle values are obtained experimentally, then interfacial tension or other parameters can be calculated.

Contact angle is typically measured on idealized and smooth surfaces but in cases where roughness at the surface is high, this roughness can impact the measurements and an effective contact angle must be defined. Note that high roughness varies by surface and fluid combinations. Cassie and Wenzel propose the use of a roughness factor  $r$ , which can be incorporated into Eq. S2 [2].

If the three interfacial tension components are known, the work of adhesion  $W_{Ad}$  can be predicted using the three interfacial properties as shown in Eq. S3 [2].

$$W_{Ad} = \gamma_{CO_2-Brine} + \gamma_{Brine-Mineral} - \gamma_{CO_2-Mineral} \quad \text{Eq. S3.}$$

The adhesion (pull-off) force  $F$  at which tensile load the adhered surfaces are separated can be calculated according to the Johnson-Kendall-Roberts (JKR) theory (Eq. S4) [3].

$$F = -1.5\pi R W_{Ad} \quad \text{Eq. S4}$$

$$R = \frac{R_{CO_2} R_{Mineral}}{R_{CO_2} + R_{Mineral}}$$

Where  $R_{CO_2}$  and  $R_{Mineral}$  are the radius of the  $CO_2$  droplet and the mineral, respectively. Work of adhesion under equilibrium states is related with equilibrium contact angle. Similarly, work of adhesion under dynamic conditions is related to the contact angle hysteresis, i.e.,

$\theta_{\text{Re}} - \theta_{\text{Ad}}$  [4, 5]. With the  $W_{\text{Re}}$  and  $W_{\text{Adv}}$  obtained from Eq. S3, The adhesion hysteresis  $\Delta W$ , shown in Eq. S5 can be determined [6].

$$\Delta W = W_{\text{Re}} - W_{\text{Adv}} \quad \text{Eq. S5}$$

Where  $W_{\text{Re}}$  and  $W_{\text{Adv}}$  are the work of adhesion during receding and advancing, respectively.

## 6 References

1. Wang, S.; Edwards, I.; Clarens, A. F., Wettability phenomena at the CO<sub>2</sub>-brinemineral interface: Implications for geologic carbon sequestration. *Environ. Sci. Technol.* **2013**, *47*, (1), 234–241; 10.1021/es301297z.
2. Churaev, N. V., Contact angles and surface forces. *Adv. Colloid Interface Sci.* **1995**, *58*, (2), 87-118;
3. Chen, C.; Zhang, D., Pore-scale simulation of density-driven convection in fractured porous media during geological CO<sub>2</sub> sequestration. *Water Resour. Res.* **2010**, *46*, (11), W11527;
4. Hong, S.-J.; Chang, F.-M.; Chou, T.-H.; Chan, S. H.; Sheng, Y.-J.; Tsao, H.-K., Anomalous Contact Angle Hysteresis of a Captive Bubble: Advancing Contact Line Pinning. *Langmuir*. **2011**, *27*, (11), 6890-6896; 10.1021/la2009418.
5. Xiu, Y.; Zhu, L.; Hess, D. W.; Wong, C. P., Relationship between work of adhesion and contact angle hysteresis on superhydrophobic surfaces. *The Journal of Physical Chemistry C*. **2008**, *112*, (30), 11403-11407;
6. Chen, Y. L.; Helm, C. A.; Israelachvili, J. N., Molecular mechanisms associated with adhesion and contact angle hysteresis of monolayer surfaces. *The Journal of Physical Chemistry*. **1991**, *95*, (26), 10736-10747;